Improved Mathematical Model for Analysis of the Payne Effect of Magnetorheological Elastomers

Si Suo[1]; Zhaodong Xu[2]; Weihua Li[3]; and Yixiang Gan, M.ASCE[4]

Abstract: Recently, magnetorheological elastomer–based vibration control devices have attracted increasing attention due to their field dependence of stiffness characteristics. It is crucial to develop a comprehensive model for precisely predicting mechanical behaviors of magnetorheological elastomers (MREs). In this work, silicon rubber–based MRE samples were prepared and investigated through dynamic and quasistatic stretch tests. Experimental results suggest that the samples possess an obvious magnetorheological effect, as well as frequency- and amplitude-dependent mechanical behavior. In order to depict these properties in a unified scheme, an extended fractional-order derivative model was developed to consider the Payne effect using the framework of the Kraus model. A comparison with experimental data indicates that this new model is accurate in predicting the mechanical behavior of MREs. **DOI: 10.1061/(ASCE)AS.1943-5525.0000868.** © *2018 American Society of Civil Engineers.*

Author keywords: Magnetorheological elastomers; Frequency-dependent behavior; Payne effect; Kraus model.

Introduction

Magnetorheological elastomers (MREs) are a new member of smart materials, whose mechanical properties can be varied by an applied magnetic field instantly, continuously, and reversibly (Cantera et al. 2017). Because of this controllability, MREs have been attracting growing interest and possess promising potential in applications relating to vibration control. Recently, an increasing number of devices based on MREs have been reported, such as building isolation systems (Behrooz et al. 2014; Li et al. 2013a, b; Yang et al. 2013), vehicle seat suspension (Du et al. 2011; Li et al. 2012), and adaptive vibration absorbers for beams (Deng and Gong 2008; Liao et al. 2014; Liao et al. 2011) and shafts (Liu et al. 2017). These devices usually operate under complex dynamic conditions across a large range of excitation amplitudes. In order to make full use of controllable properties of MREs, it is necessary to build a unified model to simultaneously consider the effects of external magnetic field, excitation frequency, and amplitude on the responses of MREs.

A variety of microscopic models have been proposed to describe the effect of an external magnetic field, i.e., the magnetorheological (MR) effect. In early studies, Jolly et al. (1996) built a dipole model considering the interaction between two adjacent particles. Davis (1999) assumed that all particles were aligned in one chain and calculated the saturated field-induced shear modulus. Shen et al. (2004) assumed that particles could be idealized as many infinite chains and took into account the interaction of all particles in one chain. These studies were based on the hypothesis of a uniform spatial distribution of particles in MRE samples. However, there is an obvious difference between this hypothesis and the real distribution of particles in anisotropic MREs due to the applied magnetic field during the matrix vulcanizing. In addition, some mathematical models considering special manufacturing techniques were proposed. For instance, Chen et al. (2007) proposed a finite-column model based on the statistical data from the SEM images. Zhang et al. (2008) developed a mathematical model that was appropriate only for the two specific kinds of particle distributions, including simple cubic and body center cubic structures. These models were developed specifically for certain types of spatial particle distributions.

At the phenomenological scale, previous studies provided parametric models to capture the measured mechanical properties of MREs. Li et al. (2010) proposed a four-parameter viscoelasticity model in which a nonlinear spring component is added to reflect the MR effect. Zhu et al. (2012) introduced a fractional-order derivative to precisely portray the viscoelastic behavior of MREs. For these two models, strain amplitudes were not considered as an independent variable, i.e., without considering Payne effects (Kraus 1971). As is well known, the Payne effect on mechanical properties of MRE cannot be ignored when MRE-based devices are applied in rather complex vibration environments. Wang et al. (2017) took large deformation into account based on a revised Bouc-Wen model. Nevertheless, the parameters of the revised Bouc-Wen model lack physical meaning and, on the contrary, this model is not suitable when MRE samples are under a small-strain excitation.

In this work, a micromechanics-enriched parametric model based on the assumption of a chi-square spatial distribution of particles was adopted to predict the mechanical behaviors of MREs that can reflect Payne effects. Then, in order to take strain amplitude (the Payne effect) into account, an improvement of the original fractional-order derivative model was introduced based on the framework of the Kraus model. In parallel, silicon rubber–based MRE samples with different contents of ferromagnetic particles were prepared and tested under quasistatic stretch and sinusoid

[1]Research Assistant, School of Civil Engineering, Univ. of Sydney, Sydney, NSW 2006, Australia. Email: si.suo@sydney.edu.au

[2]Professor, School of Civil Engineering, Southeast Univ., Nanjing 210018, P.R. China. Email: xuzhdgyq@seu.edu.cn

[3]Professor, School of Mechanical, Materials and Mechatronic Engineering, Univ. of Wollongong, Wollongong, NSW 2500, Australia. Email: weihuali@uow.edu.au

[4]Senior Lecturer, School of Civil Engineering, Univ. of Sydney, Sydney, NSW 2006, Australia (corresponding author). Email: yixiang.gan@sydney.edu.au

Note. This manuscript was submitted on October 26, 2017; approved on January 17, 2018; published online on May 19, 2018. Discussion period open until October 19, 2018; separate discussions must be submitted for individual papers. This paper is part of the ***Journal of Aerospace Engineering***, © ASCE, ISSN 0893-1321.

excitation, and the proposed parametric model was then validated by comparing with the experimental data.

Experiments

Sample Preparation

Because of its lower hardness, silicon rubber is usually chosen as the matrix material of MREs, allowing a rather wide range of controllable stiffnesses. Thus, this study used HTV-type methyl-vinyl silicon rubber as the matrix of samples. Carbonyl iron powder of 2.5-μm diameter was taken as filling ferromagnetic particles. The other compositions of the samples are given in Table 1. In this work, two samples were prepared, named Q60 and Q70, respectively, according to the content of ferromagnetic powder.

The whole manufacturing procedure included three steps: (1) mixing the additives with silicon rubber homogeneously on a two-roll mill step by step at room temperature; (2) filling a mold with the mixture and curing the material in a plate-type vulcanizing machine under a pressure of 15 MPa at 165°C for 30 min and appling 100-mT external magnetic field during the whole process; and (3) forming the MRE samples into sandwich-type specimens, as shown in Fig. 1.

Table 1. Compositions of MRE samples

Composition	Content (phr)
Silicon rubber	100
Carbonyl iron powder	60/70
White carbon black	20
Methyl silicone oil	15
DCP	2
CTP	5

Note: CTP = C14H15O2NS; DCP = Dicumyl Peroxide; and phr = parts per hundreds of rubber.

Test Procedure

In order to systematically investigate the mechanical properties of MREs, the quasistatic and dynamic experiments were carried out on a mechanical testing system (MTS) loading frame as shown in Fig. 2.

In the quasistatic tests, MRE samples Q60 and Q70 were stretched under the magnetic fields of 0 and 150 mT measured by a magnetometer, as shown in Fig. 2(d), with a given stretching rate of 0.1 mm/s and final stretching distance of 4 mm. However, the real stretching rate did not follow the setting value exactly due to the issue of equipment precision. The mean shear rate was calculated by using the actual stretching time and it is given in Table 2.

In the dynamic experiments, various sinusoidal excitations are applied to the MRE specimens under different magnetic fields, and the test conditions can be seen in Table 3. The load-displacement hysteresis curve obtained from dynamic experimental data is a typical elliptical curve, and important parameters including the shear storage modulus G_1 and shear loss modulus G_2 can be calculated according to classic viscoelasticity theory (Cho 2016) as

$$G_1 = \frac{F_1 \cdot t_v}{u_0 \cdot m_v \cdot A_v} \tag{1}$$

$$G_2 = \frac{F_2}{F_1} \cdot G_1 \tag{2}$$

where m_v = number of MRE layers; t_v and A_v = thickness and area of the MRE layer, respectively; u_0 = excitation amplitude; F_1 = force when the displacement reaches maximum; and F_2 = force when the displacement is zero.

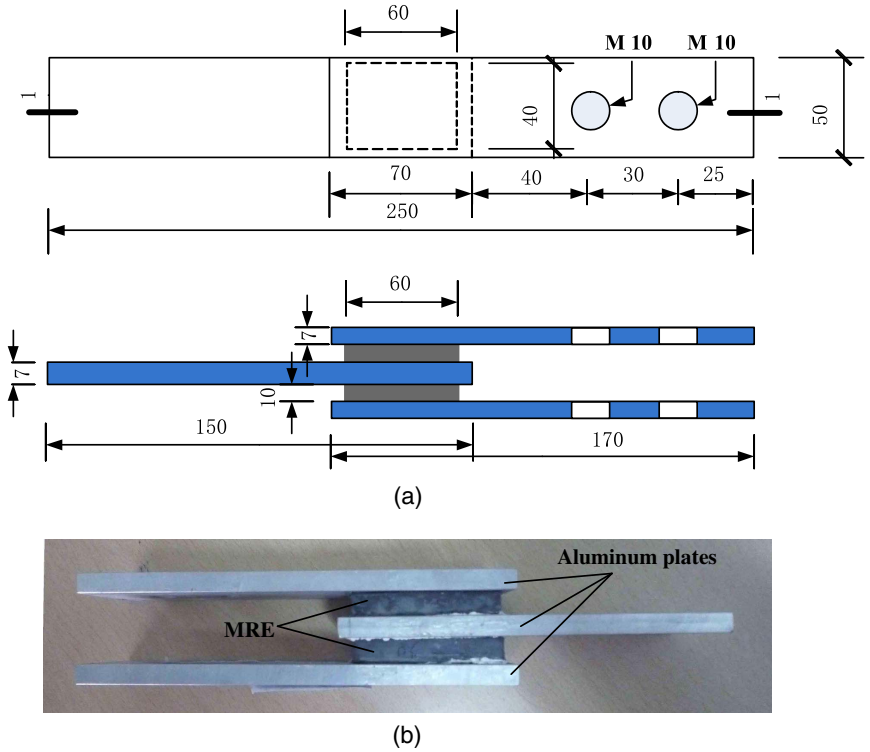

Fig. 1. (a) Schematics of the MRE specimen containing MRE with dimensions in millimeters; and (b) photo of the MRE specimen, image by authors.

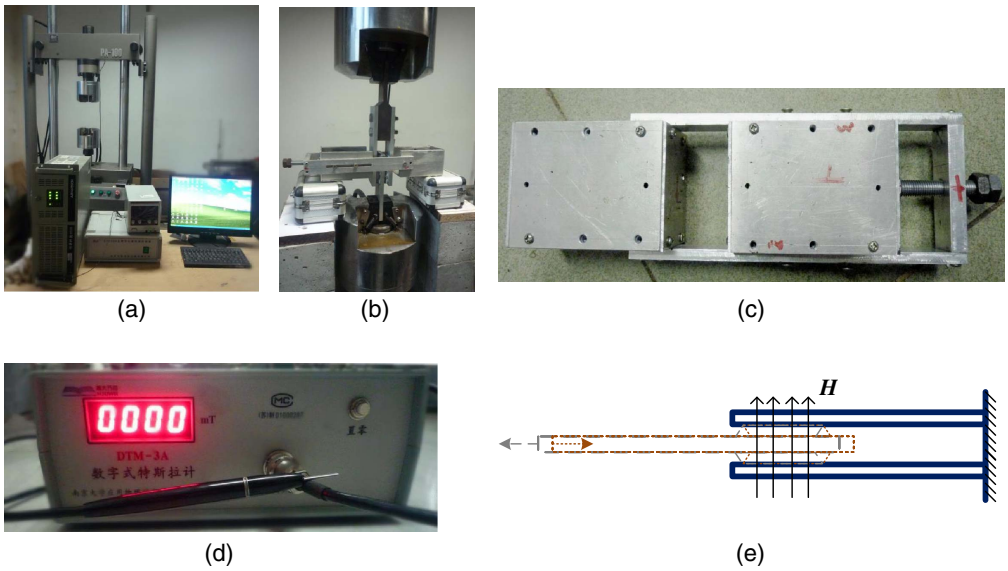

Fig. 2. Experimental setup: (a) MTS loading frame; (b) details of the load cell; (c) the magnetic field apparatus; (d) Tesla magnetometer; and (e) schematic of loading condition. (Images by authors.)

Table 2. Stretching time and mean shear rate in quasistatic tests

	Stretching time (s)		Mean shear rate (1/s)	
Specimens	0 mT	150 mT	0 mT	150 mT
Q60	96.9	66.5	0.0041	0.0060
Q70	245.8	238.3	0.0016	0.0017

Note: Mean shear rate = ratio of total shear strain to stretching time.

Table 3. Dynamic test conditions

Number	External magnetic field (mT)	Displacement (mm)	Frequency (Hz)
1	0	1, 2, 3	0.3, 0.5, 1.0, 1.5, 2.0
2	50	1, 2, 3	0.3, 0.5, 1.0, 1.5, 2.0
3	100	1, 2, 3	0.3, 0.5, 1.0, 1.5, 2.0
4	150	1, 2, 3	0.3, 0.5, 1.0, 1.5, 2.0

Experimental Results

As for quasistatic tests, the stress-strain curves of Q60 and Q70 are shown in Figs. 3(a and b), respectively. For both cases, the shear modulus decreases with respect to the shear strain when strain is below 0.2 and then stays almost a constant; compared with zero external magnetic field condition, the tangent modulus presents an obvious raise with an applied external magnetic field.

Through dynamic tests, the influence of external magnetic field, excitation frequency, and amplitude were investigated independently. As for the external magnetic field, the conditions of 5 Hz and 1 mm under different magnetic intensities (0, 50, 100, and 150 mT) are compared in Fig. 4. The shear storage modulus G_1 increases with the external magnetic field for both MRE samples Q60 (10.0% increment at 150 mT) and Q70 (7.3% at 150 mT), while there is only a slight raise (<5%) in the shear loss modulus G_2 compared with G_1.

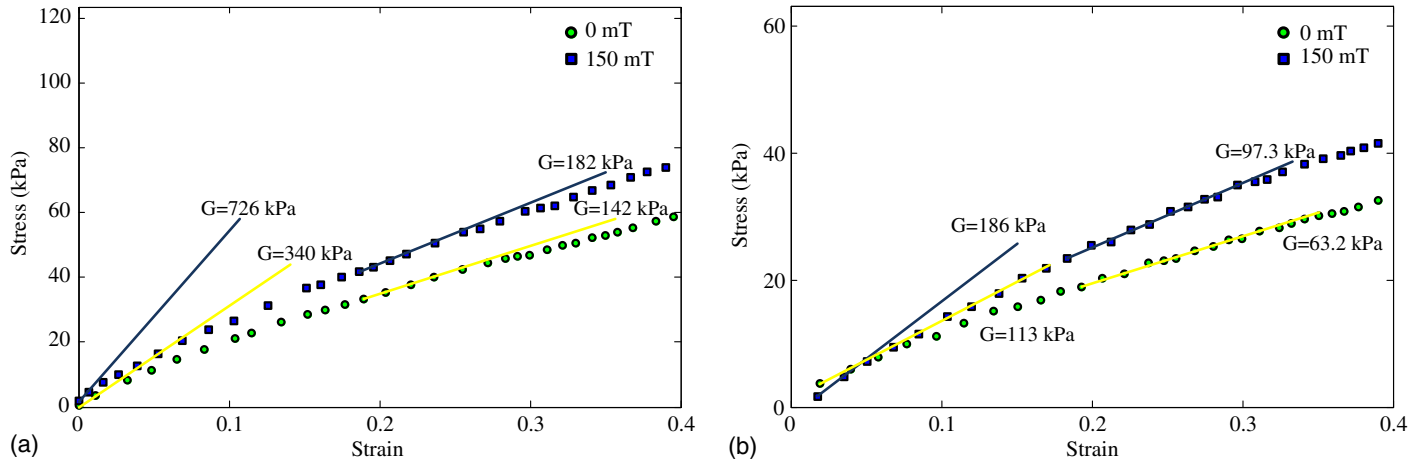

Fig. 3. Shear stress-strain curves during quasistatic tests under different magnetic fields: (a) Q60; and (b) Q70.

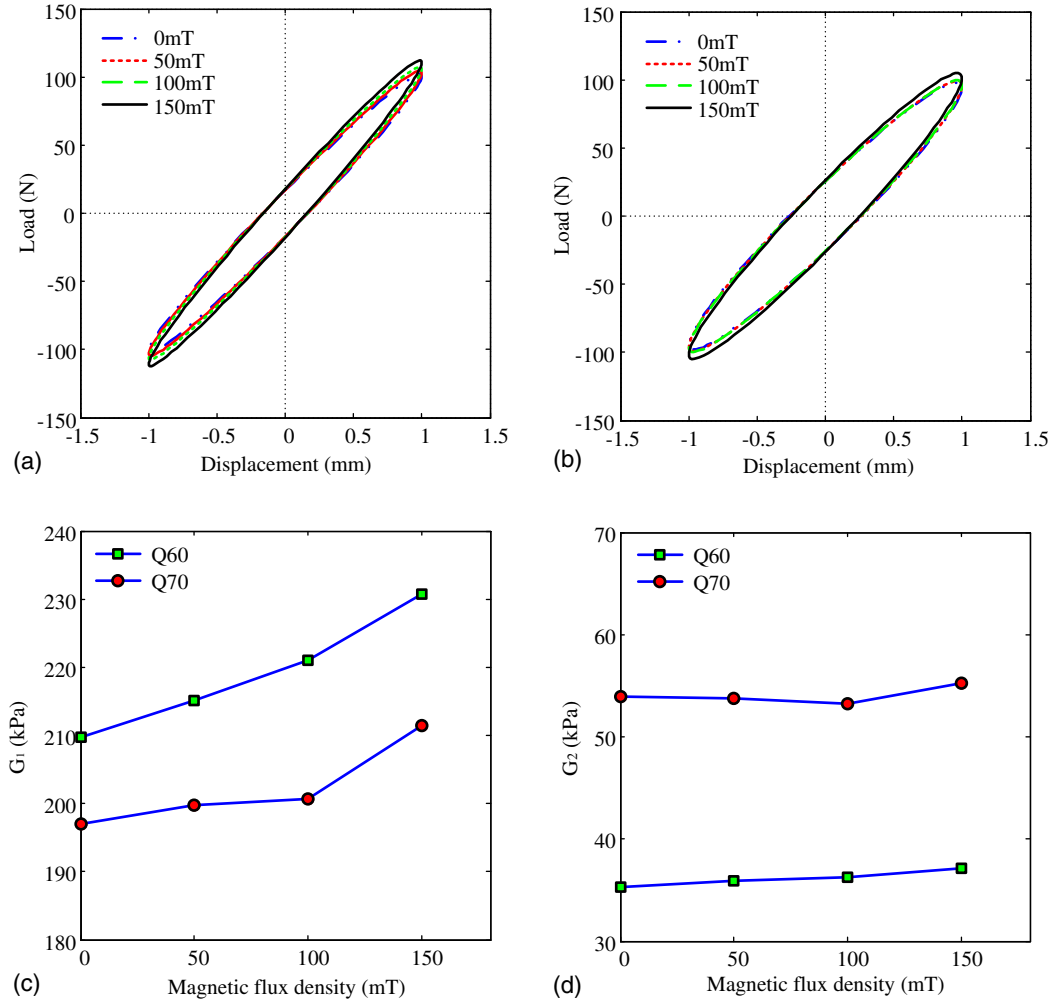

Fig. 4. Load-displacement loops: (a) Q60 and (b) Q70, with shear moduli of MRE samples; (c) G_1 and (d) G_2 under different magnetic fields.

In order to clarify the effects of the excitation frequency on the storage modulus G_1 and loss modulus G_2, test data with an amplitude of 1 mm and external magnetic field of 150 mT were extracted, as shown in Fig. 5. For both MREs, shear storage moduli of Q60 and Q70 increased with excitation frequency and had similar tendencies. More specifically, G_1 rose noticeably in the low-frequency range (≤1.0 Hz), while it became less sensitive to frequencies higher than 1.5 Hz; compared to G_1, G_2 increased significantly in the whole tested frequency range. In summary, MRE samples present typical viscoelasticity properties, i.e., frequency-dependent behavior.

Similarly, the effects of the excitation amplitude on MRE samples were investigated and are shown in Fig. 6, in which the test data with an excitation frequency of 1 Hz and magnetic field of 100 mT are plotted. For both Q60 and Q70, the shear storage modulus drops sharply with an excitation amplitude from 1 to 3 mm, while the shear loss modulus decreases moderately. This suggests that the mechanical properties of MRE samples are amplitude dependent, i.e., Payne effects.

In accordance with the above results and discussions, it can be concluded that the mechanical behavior of MRE samples is determined by external magnetic field and excitation frequency and amplitude. Thus, a unified model should be developed to simultaneously consider all of these effects.

Modeling

Microscopic Scale

Generally, the difficulty of modeling on MREs lies in how to precisely and concisely describe spatial distribution of particles. Here, a microphysical model based on chi-squared distribution (Xu et al. 2018) was adopted to describe the effect of external magnetic fields, and the magnetic-induced shear modulus G_m can be expressed as

$$G_m = \frac{\phi \cdot (4-\varepsilon^2) \cdot J_p^2}{8\mu_1\mu_0 \cdot (\varepsilon^2+1)^{7/2}} \cdot g(n) \tag{3}$$

where ϕ = volume fraction of the particles; ε = shear strain; μ_0 = vacuum permeability and μ_1 = relative permeability of the medium; and n = distribution parameter that can reflect the average level of adjacent particle distance. The dipole moment magnitude J_p is determined by external magnetic field intensity H and the relationship between these two quantities for the ferromagnetic particles used in this work was measured through a vibrating sample magnetometer (VSM). As can be seen in Fig. 7, J_p is proportional to H when the absolute value of H is less than 130 kA/m and the scale factor is 0.0096 T/(kA/m), while the ferromagnetic particles are in magnetic saturation, and J_p reaches

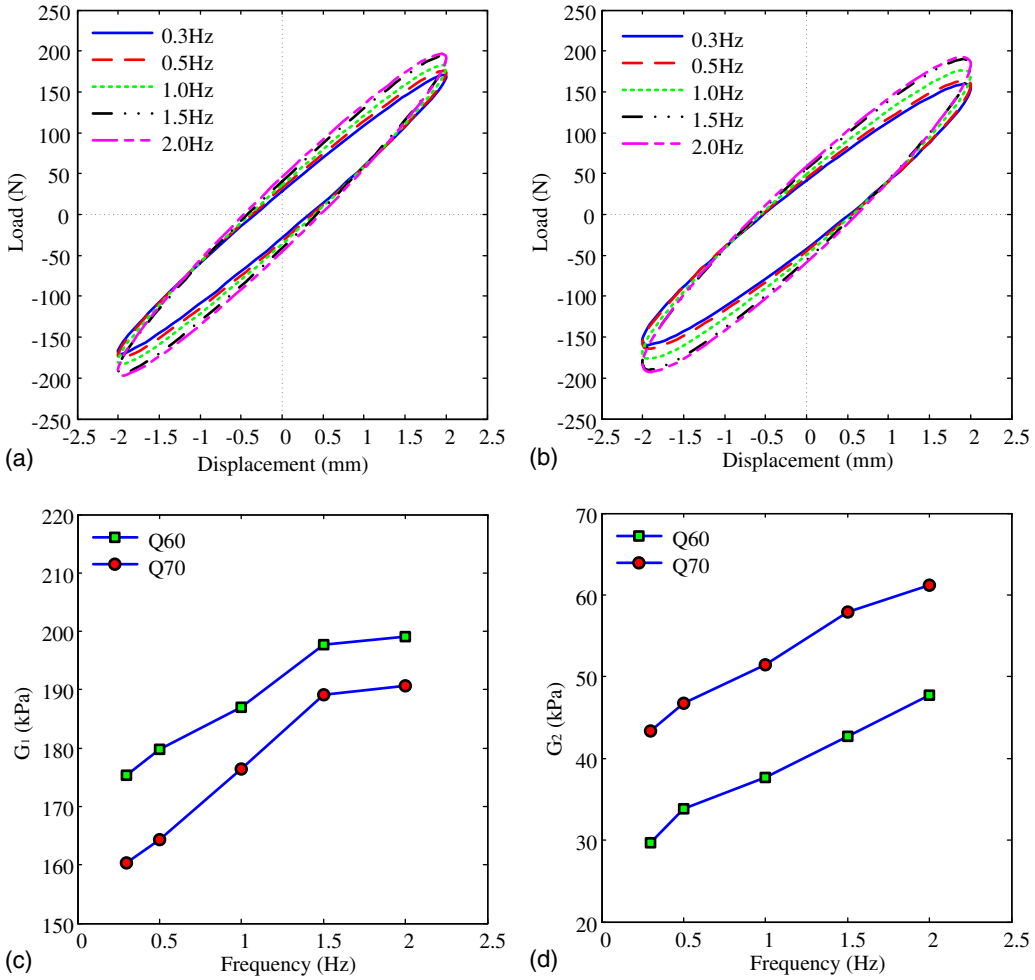

Fig. 5. Load-displacement loops: (a) Q60 and (b) Q70, with shear moduli of MRE samples; (c) G_1 and (d) G_2 under different excitation frequencies.

the maximum value of 2.14 T when the absolute value of H is beyond 350 kA/m.

In order to describe the phenomenological behavior of MREs, i.e., the relationship between force and displacement or stress and strain, it is necessary to propose a macroscopic model based on Eq. (3), in which G_m can be used as the magnetic-induced part.

Macroscopic Scale

The fractional derivative model has been widely used in describing the viscoelastic behavior of materials in time and frequency domain (Zhu et al. 2012). Together with the microscopic physical model, a more appropriate scheme is proposed in this work as follows.

As shown in Fig. 8, the storage modulus G_1 and the loss modulus G_2 can be expressed as

$$G_1 = G_m + G_c + \eta_c \cdot \omega^{\alpha} \cdot \cos\left(\frac{\alpha\pi}{2}\right) \tag{4}$$

$$G_2 = \omega \cdot \mu \cdot G_m + \eta_c \cdot \omega^{\alpha} \cdot \sin\left(\frac{\alpha\pi}{2}\right) \tag{5}$$

where G_c = static shear modulus, which determines the elastic component; η_c = viscosity coefficient and α = fractional order, both of which determine the viscous component; G_m can be obtained according to Eq. (3), $f(G_m)$ = additional damping due to external magnetic fields, and these two components describe the magnetic-induced behavior; and ω = angular frequency. The additional damping is assumed to be proportional to G_m as $f(G_m) = \mu \cdot G_m$.

In accordance with Eqs. (4) and (5), this existing fractional derivative model can take the excitation frequency and external magnetic field into account, but the model obviously excludes the influence of strain amplitude, which is also an important factor according to the experimental results, shown in the section "Experiments." Therefore, a modification is proposed as follows based on the Kraus model.

From experimental data, the behavior of MRE samples demonstrates a clear amplitude dependency, i.e., the so-called Payne effect, which can be explained and modeled by the classical Kraus model. In order to couple the Kraus model with macroscopic parametric model of MREs, it is modified firstly as follows. In the Kraus model, the breaking function f_b and rebuilding function f_r are both in the form of an exponent with the same index m. However, filling particles in MRE may form additional van der Waals interactions and provide more friction, which results in a different influence on the breaking and rebuilding processes. Therefore, it can be assumed that

$$f_b(\varepsilon_0) = \varepsilon_0^{m_1}, \qquad f_r(\varepsilon_0) = \varepsilon_0^{-m_2} \tag{6}$$

where m_1 and m_2 = breaking factor and rebuilding factor, respectively. Then, following the Kraus modeling scheme, the storage

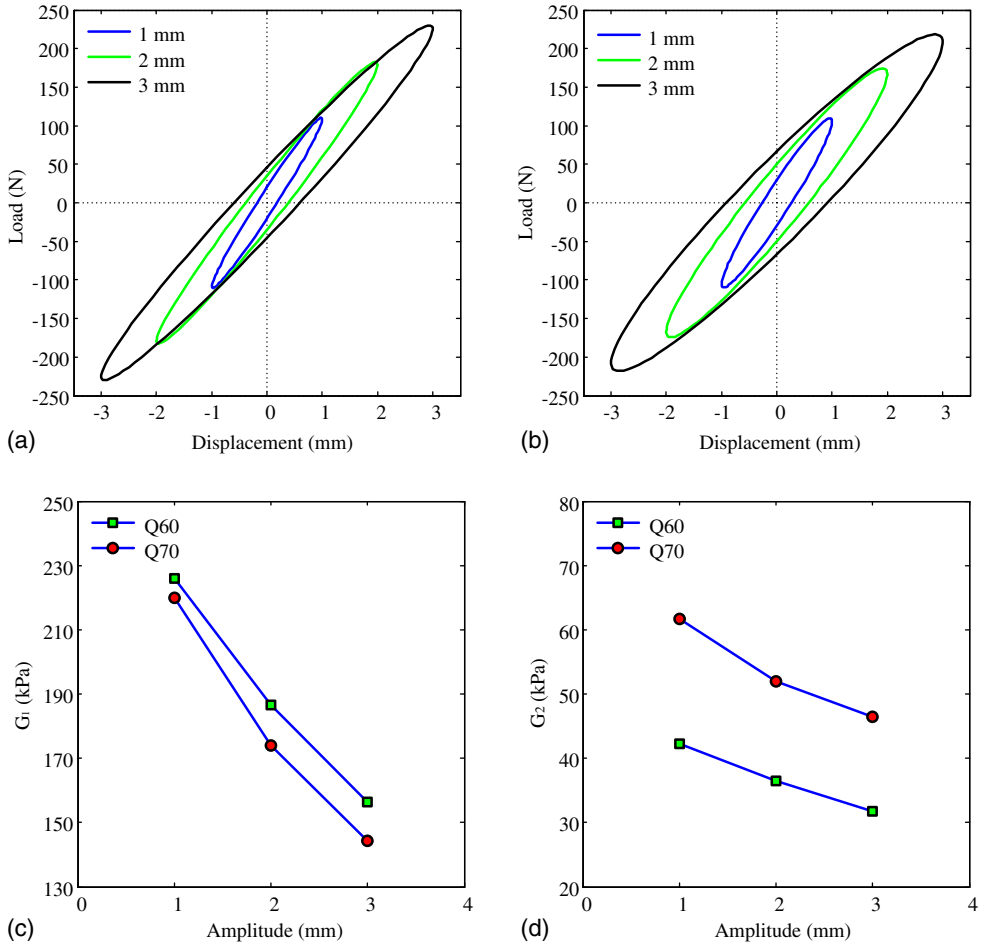

Fig. 6. Load-displacement loops: (a) Q60 and (b) Q70, with shear moduli of MRE samples; (c) G_1 and (d) G_2 under different excitation amplitudes.

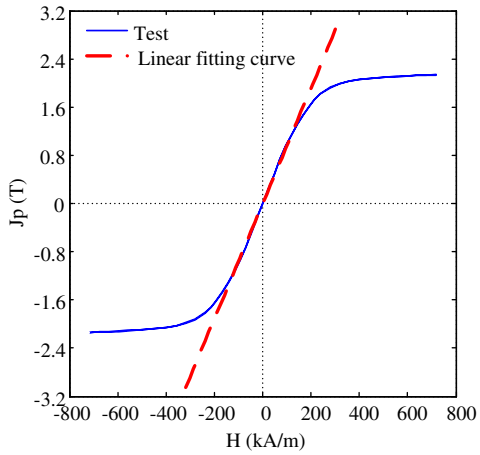

Fig. 7. Relationship between dipole moment magnitude and external magnetic field intensity.

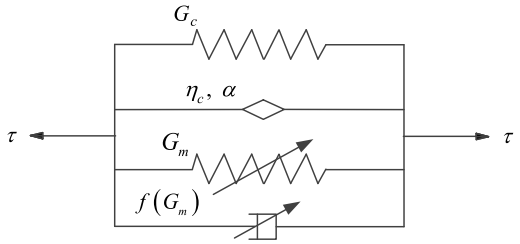

Fig. 8. Schematic of the fractional derivative model.

modulus $G_1(\omega,\varepsilon_0)$ and loss modulus $G_2(\omega,\varepsilon_0)$, at any strain amplitude ε_0, can be derived as

$$G_1(\omega,\varepsilon_0)=[G_1(\omega,0)-G_1(\omega,\infty)]\cdot\frac{1}{1+(\varepsilon_0/\varepsilon_c)^{m_1+m_2}}+G_1(\omega,\infty) \tag{7}$$

$$G_2(\omega,\varepsilon_0)=[G_2(\omega,\varepsilon_c)-G_2(\omega,\infty)]\cdot\frac{2(\varepsilon_0/\varepsilon_c)^{m_1}}{1+(\varepsilon_0/\varepsilon_c)^{m_1+m_2}}+G_2(\omega,\infty) \tag{8}$$

where ε_c is a constant and its physical meanings can be referred (Kraus 1971).

For simplicity, we assume that $G_1(\omega,\infty)=b_1$ and $G_2(\omega,\infty)=b_2$ are both constants; $G_1(\omega,0)-G_1(\omega,\infty)=k_1\cdot G_1$ and $G_2(\omega,\varepsilon_c)-G_2(\omega,\infty)=k_2\cdot G_2$, where k_1 and k_2 are proportional coefficients; G_1 and G_2 can be referred to Eqs. (4) and (5). Thus, considering the Payne effect, the fractional derivative model can be modified as

$$G_1=k_1\cdot\left[G_m+G_c+\eta_c\cdot\omega^{\alpha}\cdot\cos\left(\frac{\alpha\pi}{2}\right)\right]\Big/[1+(\varepsilon_0/\varepsilon_c)^{m_1+m_2}]+b_1 \tag{9}$$

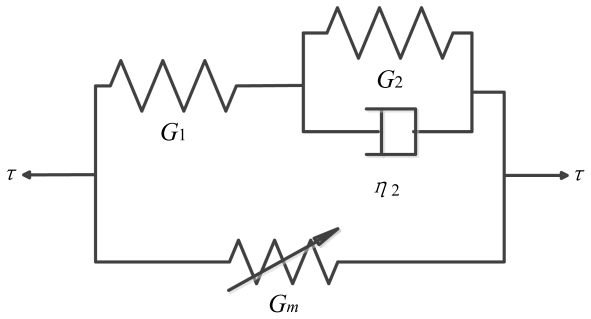

Fig. 9. Three-parameter solid model.

Table 4. Quasistatic model parameters of Q60 and Q70

Sample	Parameters			
	q_0 (kPa)	q_1 (kPa · s)	p_1 (s)	n
Q60	113.74	5,771.9	21.56	1.8542
Q70	68.13	6,101.6	33.91	2.5873

$$G_2 = k_2 \cdot \left[\omega \cdot \mu \cdot G_m + \eta_c \cdot \omega^{\alpha} \cdot \sin\left(\frac{\alpha\pi}{2}\right)\right] \cdot \frac{2(\varepsilon_0/\varepsilon_c)^{m_1}}{1+(\varepsilon_0/\varepsilon_c)^{m_1+m_2}} + b_2 \quad (10)$$

In summary, parameters in this model include the fractional derivative model parameters, G_c, η_c, α, and μ; modified Kraus model parameters, ε_c, m_1, and m_2; and linear parameters, k_1, b_1, k_2, and b_2. Also, the distribution parameter n in the microscopic physical model should be included, and it can be identified as follows according to the quasistatic test results and three-parameter solid model, as shown in Fig. 9.

Assuming strain γ is linearly proportional to loading time t, i.e., $\gamma = k \cdot t$, then total stress τ can be solved as

$$\tau = k \cdot (q_0 \cdot p_1 - q_1) \cdot [e^{-\gamma/(k \cdot p_1)} - 1] + q_0 \cdot \gamma + G_m \cdot \gamma \quad (11)$$

where q_0, p_1, and q_1 = undetermined coefficients; G_m = magnetic-induced shear modulus, which can be referred to the microscopic model shown in Eq. (3). Then, the least-squares method is adopted according to the error formulation as follows:

$$\delta = \sum_{i=1}^{m} [\tau_M(i) - \tau_E(i)]^2 \quad (12)$$

where τ_M = model value; τ_E = experimental results; and m = total number of experimental cases. The identified model parameters are shown in Table 4 and comparisons between the experiment and model are shown in Fig. 10.

For predicting the dynamic tests, the distribution parameter n of two samples is obtained previously from the quasistatic tests, as shown in Table 4, while the other model parameters can be identified according to the proposed macroscopic parametric model. The error formulation is the same as that above Eq. (12), where τ_M can be expressed as

$$\tau_M = \varepsilon_0 \cdot \sqrt{G_1^2 + G_2^2}\sin(\omega \cdot t + \varphi) \quad (13)$$

where φ = phase difference $\varphi = \tan^{-1}(G_2/G_1)$; and ε_0 = strain amplitude. The model parameters are listed in Table 5. The proposed model fits the experimental data very well through the comparison shown in Fig. 11, and the errors between experimental data and model value for Q60 and Q70 are less than 7.3 and 9.9%, respectively.

As can be seen in Fig. 11, the predictions of the proposed mathematical model fit well with the experimental data; i.e., it can portray the mechanical properties of MREs, in particular accurately capturing the dependency on the excitation amplitude. Here, only typical results under two magnetic fields (0 and 150 mT) are shown, and the comparison with other cases demonstrates similar trends.

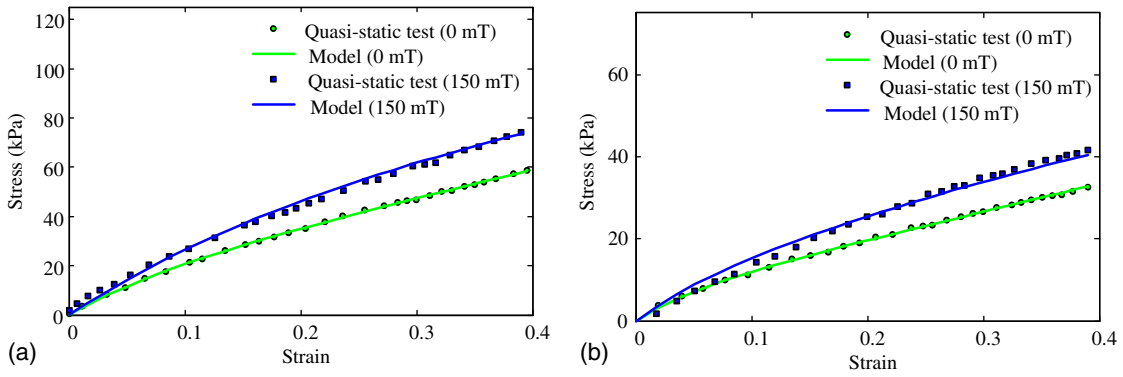

Fig. 10. Comparison between quasistatic tests and model predictions: (a) Q60; and (b) Q70.

Table 5. Parameters of macroscopic parametric model

Samples	Fractional derivative model parameters				Modified Kraus model parameters			Linear parameters			
	G_c[a] (kPa)	η_c[a] (kPa · s$^{\alpha}$)	α[a]	μ (s)	ε_c	m_1	m_2	k_1	b_1	k_2	b_2
Q60	270.25	53.5	0.4	0.05	0.098	0.03	0.87	0.78	80.0	0.3	21.0
Q70	199.35	70.7	0.6	0.03	0.101	0.01	1.09	0.80	85.3	0.16	33.6

[a]Identified based on the cases without external magnetic fields only.

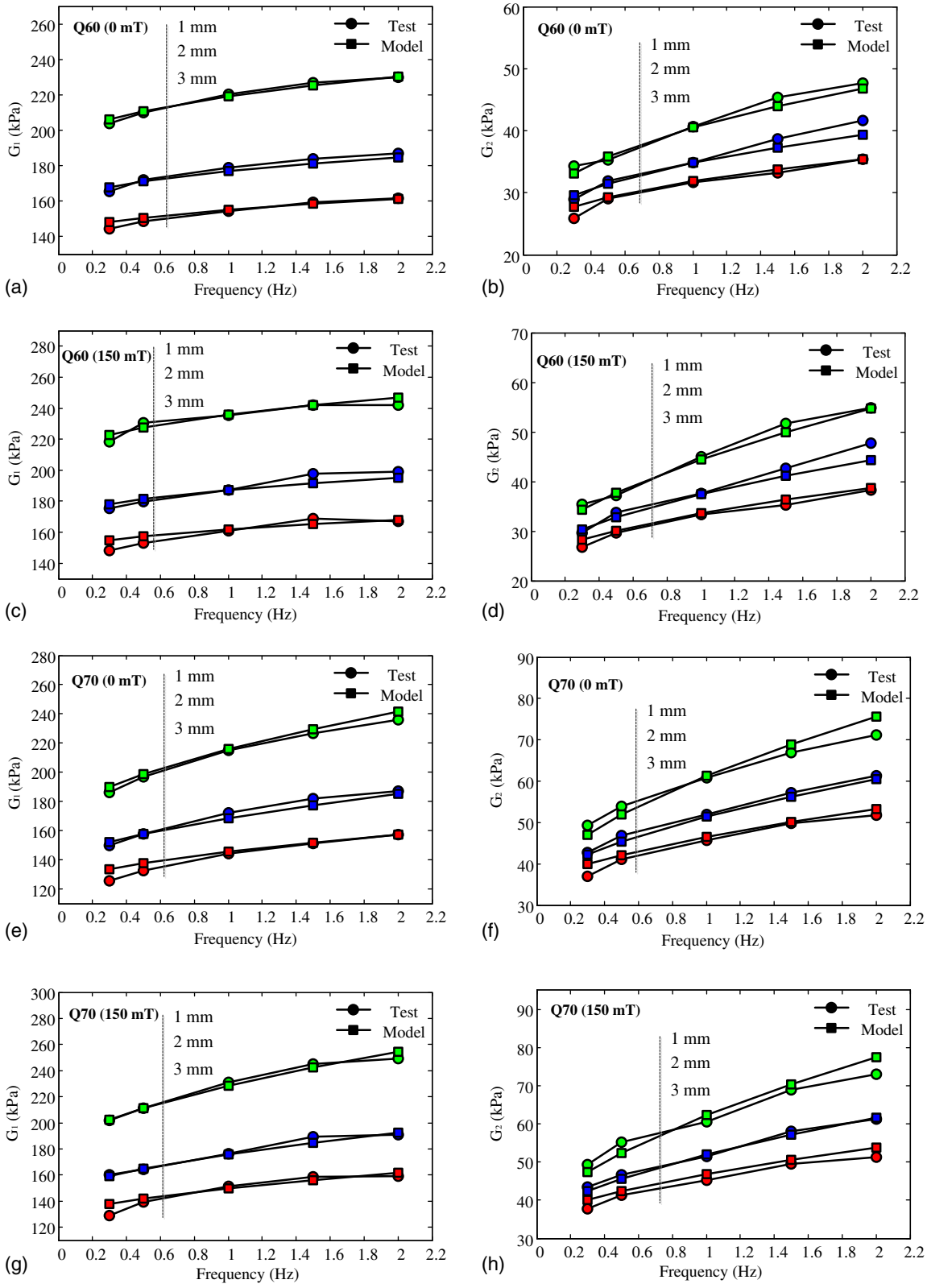

Fig. 11. Comparison between dynamic test results and model predictions for the shear storage and shear loss moduli (left and right columns, respectively) under different excitation amplitudes (1, 2, and 3 mm from top to bottom in each subfigure): (a and b) Q60 (0 mT); (c and d) Q60 (150 mT); (e and f) Q70 (0 mT); and (g and h) Q70 (150 mT).

Conclusions

In this paper, we proposed a micromechanics-enriched model that can predict the MR effect of MREs exactly in a simple formation, and then the existing fractional-order derivative model was improved based on the Kraus model in order to consider the Payne effect. Combining the above theoretical approaches, we developed a unified parametric model that can reflect the MR effect, as well as

the frequency- and amplitude-dependent mechanical properties of MREs.

The validation of the proposed model was conducted through comparing the model predictions with quasistatic and dynamic test results of silicon rubber–based MRE samples. This model is suitable and applicable as long as the load-displacement loops of MRE samples keep an elliptic shape; i.e., no unrecoverable deformation occurs in MRE samples. Because of the experimental limitation, the external magnetic field is smaller compared with saturate carbonyl iron powder in MRE samples, so future work should also focus on the effect of magnetic saturation on the mechanical properties of MREs.

References

Behrooz, M., X. Wang, and F. Gordaninejad. 2014. "Modeling of a new semi-active/passive magnetorheological elastomer isolator." *Smart Mater. Struct.* 23 (4): 045013. https://doi.org/10.1088/0964-1726/23/4/045013.

Cantera, M. A., M. Behrooz, R. F. Gibson, and F. Gordaninejad. 2017. "Modeling of magneto-mechanical response of magnetorheological elastomers (MRE) and MRE-based systems: A review." *Smart Mater. Struct.* 26 (2): 023001. https://doi.org/10.1088/1361-665X/aa549c.

Chen, L., X. Gong, and W. Li. 2007. "Microstructures and viscoelastic properties of anisotropic magnetorheological elastomers." *Smart Mater. Struct.* 16 (6): 2645–2650. https://doi.org/10.1088/0964-1726/16/6/069.

Cho, K. S. 2016. *Viscoelasticity of polymers*. New York: Springer.

Davis, L. C. 1999. "Model of magnetorheological elastomers." *J. Appl. Phys.* 85 (6): 3348–3351. https://doi.org/10.1063/1.369682.

Deng, H.-X., and X.-L. Gong. 2008. "Application of magnetorheological elastomer to vibration absorber." *Commun. Nonlinear Sci. Numer. Simul.* 13 (9): 1938–1947. https://doi.org/10.1016/j.cnsns.2007.03.024.

Du, H., W. Li, and N. Zhang. 2011. "Semi-active variable stiffness vibration control of vehicle seat suspension using an MR elastomer isolator." *Smart Mater. Struct.* 20 (10): 105003. https://doi.org/10.1088/0964-1726/20/10/105003.

Jolly, M. R., J. D. Carlson, and B. C. Munoz. 1996. "A model of the behaviour of magnetorheological materials." *Smart Mater. Struct.* 5 (5): 607–614. https://doi.org/10.1088/0964-1726/5/5/009.

Kraus, G. 1971. "Reinforcement of elastomers by carbon black." In *Fortschritte der Hochpolymeren-Forschung*, 155–237. New York: Springer.

Li, W. H., X. Zhang, and H. Du. 2012. "Development and simulation evaluation of a magnetorheological elastomer isolator for seat vibration control." *J. Intell. Mater. Syst. Struct.* 23 (9): 1041–1048. https://doi.org/10.1177/1045389X11435431.

Li, W. H., Y. Zhou, and T. F. Tian. 2010. "Viscoelastic properties of MR elastomers under harmonic loading." *Rheol. Acta* 49 (7): 733–740. https://doi.org/10.1007/s00397-010-0446-9.

Li, Y., J. Li, W. Li, and B. Samali. 2013a. "Development and characterization of a magnetorheological elastomer based adaptive seismic isolator." *Smart Mater. Struct.* 22 (3): 035005. https://doi.org/10.1088/0964-1726/22/3/035005.

Li, Y., J. Li, T. Tian, and W. Li. 2013b. "A highly adjustable magnetorheological elastomer base isolator for applications of real-time adaptive control." *Smart Mater. Struct.* 22 (9): 095020. https://doi.org/10.1088/0964-1726/22/9/095020.

Liao, G., X. Gong, and S. Xuan. 2014. "Phase based stiffness tuning algorithm for a magnetorheological elastomer dynamic vibration absorber." *Smart Mater. Struct.* 23 (1): 015016. https://doi.org/10.1088/0964-1726/23/1/015016.

Liao, G. J., X. L. Gong, C. J. Kang, and S. H. Xuan. 2011. "The design of an active–adaptive tuned vibration absorber based on magnetorheological elastomer and its vibration attenuation performance." *Smart Mater. Struct.* 20 (7): 075015. https://doi.org/10.1088/0964-1726/20/7/075015.

Liu, G., K. Lu, D. Zou, Z. Xie, Z. Rao, and N. Ta. 2017. "Development of a semi-active dynamic vibration absorber for longitudinal vibration of propulsion shaft system based on magnetorheological elastomer." *Smart Mater. Struct.* 26 (7): 075009. https://doi.org/10.1088/1361-665X/aa73f3.

Shen, Y., M. F. Golnaraghi, and G. R. Heppler. 2004. "Experimental research and modeling of magnetorheological elastomers." *J. Intell. Mater. Syst. Struct.* 15 (1): 27–35. https://doi.org/10.1177/1045389X04039264.

Wang, Q., X. Dong, L. Li, and J. Ou. 2017. "A nonlinear model of magnetorheological elastomer with wide amplitude range and variable frequencies." *Smart Mater. Struct.* 26 (6): 065010. https://doi.org/10.1088/1361-665X/aa66e3.

Xu, Z.-D., S. Suo, J.-T. Zhu, and Y.-Q. Guo. 2018. "Performance tests and modeling on high damping magnetorheological elastomers based on bromobutyl rubber." *J. Intell. Mater. Syst. Struct.* 29 (6): 1025–1037. https://doi.org/10.1177/1045389X17730909.

Yang, J., H. Du, W. Li, Y. Li, J. Li, S. Sun, and H. X. Deng. 2013. "Experimental study and modeling of a novel magnetorheological elastomer isolator." *Smart Mater. Struct.* 22 (11): 117001. https://doi.org/10.1088/0964-1726/22/11/117001.

Zhang, X., S. Peng, W. Wen, and W. Li. 2008. "Analysis and fabrication of patterned magnetorheological elastomers." *Smart Mater. Struct.* 17 (4): 045001. https://doi.org/10.1088/0964-1726/17/4/045001.

Zhu, J.-T., Z.-D. Xu, and Y.-Q. Guo. 2012. "Magnetoviscoelasticity parametric model of an MR elastomer vibration mitigation device." *Smart Mater. Struct.* 21 (7): 075034. https://doi.org/10.1088/0964-1726/21/7/075034.